Plasma Chemistry and Plasma Processing, Vol. 15, No. 3, 1995

Effect of Power Modulation on Radical Concentration and Uniformity in a Single-Wafer Plasma Reactor

Ping Jiang,[1] Demetre J. Economou,[1,3] and Chee Burm Shin[2]

Received January 27, 1994; revised October 11, 1994

The effect of power modulation on radical concentration and uniformity in a single-wafer plasma reactor was investigated with a radical transport and reaction model. Plasma etching of silicon using tetrafluoromethane under relatively high pressure (~1 torr) high frequency (13.56 MHz) conditions was taken as an example system. Gas velocity, temperature, and radical concentration profiles were obtained numerically by a finite element method. When compared to a continuous wave plasma, power modulation can alter the relative concentration of radicals and in turn the etch rate and uniformity as well as selectivity and anisotropy. Uniformity is improved by power modulation except at high flow rates which, however, result in poor utilization of the feedstock gas.

KEY WORDS: Power modulation; mathematical model; uniformity; pulsed discharge; tetrafluoromethane plasma; silicon etching; finite elements.

1. INTRODUCTION

Etching and deposition of thin films using reactive gas plasmas are important operations in the fabrication of microelectronic devices.[1] Plasma processing offers the advantage of low gas temperature and, in the case of etching, submicron pattern resolution by the action of energetic ion bombardment. The goal of plasma etching is to achieve rapid and damage-free film removal while at the same time preserving uniformity, anisotropy, and selectivity. Etching nonuniformity is frequently encountered in plasma reactors, especially in magnetically enhanced systems. Uniformity problems may become worse as wafer size increases and new gas formulations yielding faster reaction rate are developed. Etch nonuniformity may be the result of

[1]Plasma Processing Laboratory, Department of Chemical Engineering, University of Houston, Houston, Texas 77204-4792.
[2]Department of Chemical Engineering, Ajou University, Suwon 441-749, S. Korea.
[3]To whom correspondence should be addressed.

0272-4324/95/0900 0383$07.50/0 © 1995 Plenum Publishing Corporation

gradients in etchant concentration, ion bombardment flux and/or energy, or wafer surface temperature.[2,3]

Etch anisotropy frequently depends on the deposition of thin polymer films on the sidewalls of the feature. These films act as protective layers preventing etching of the sidewall. In contrast, the bottom of the feature is kept reactive by the action of directional ion bombardment which removes any polymer deposits, or prevents their formation. The formation of protective polymeric films is promoted by unsaturated radicals formed in the plasma. For example, CF_2 radicals are known to promote polymer deposition in fluorocarbon-based plasmas.[4] Polymer deposition is also the mechanism of enhanced selectivity of etching SiO_2 over Si. There is a fine balance between etching and gross polymerization in these systems governed by the relative abundance of unsaturated radicals such as CF_2 compared to free F and CF_3 radicals.[5]

Many factors can affect the radical concentration and its distribution in a plasma reactor; for example, pressure, power, flow rate, reactor design and wall materials, excitation frequency, etc. Recently, a new method for controlling the concentration of certain radicals relative to other radicals has been proposed in an effort to influence selectivity and anisotropy. This method involves modulation of the power delivered to the plasma. For example, Samukawa and Furuoya[6] as well as Takahashi *et al.*[7] used the power modulation technique to control the relative abundance of CF_x radicals in a CHF_3 plasma. In other applications, pulsed plasmas have been used to extract negative ions during the power-off fraction of the cycle,[8,9] to reduce particulate formation in silane discharges,[10–13] to measure the lifetime of important radicals in the plasma,[14,15] and to improve the reaction uniformity in plasma CVD and etching.[16]

Power modulation can influence not only the relative concentration of radicals, but also the spatial distribution of these radicals in the plasma reactor. For example, as the gas flows through the plasma, the gas is depleted by electron-impact dissociation. As a result, the etch or deposition rate can vary greatly along the flow path of the gas.[16] Power modulation can be used to alleviate these rate variations and therefore improve uniformity. Let us take an example system in which the power delivered to the plasma is modulated according to a square waveform (Fig. 1). The frequency of the applied power (e.g., 13.56 MHz) is much higher than the frequency of the square-wave modulation (e.g., 100 Hz). There are two mechanisms by which power modulation as shown in Fig. 1a can affect the spatial distribution of radicals: (1) if the plasma is switched off for a period of time comparable to the gas residence time, the reactor can be essentially refilled with fresh gas during that period of time. This minimizes spatial density variations of the parent gas and in turn improves uniformity. (2) if the plasma is switched

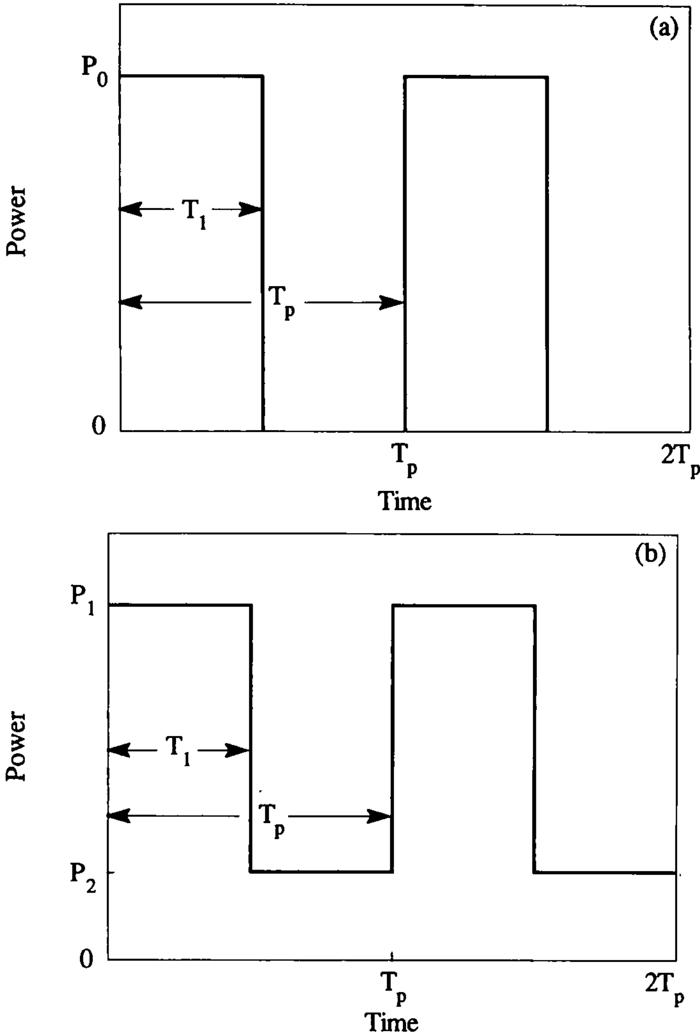

Fig. 1. Square-wave modulation of power input to the plasma: (a) full modulation, and (b) partial modulation. The duty cycle is defined as $f_d = T_1/T_p$.

off before appreciable concentration gradients of key radicals can be established, this will again improve uniformity.

In the present work, the effect of power modulation on radical concentration, spatial distribution of radicals, etch rate, and uniformity was investigated. The etching of silicon using tetrafluoromethane gas was taken as an example system. The relative concentration variations of CF_x radicals as a

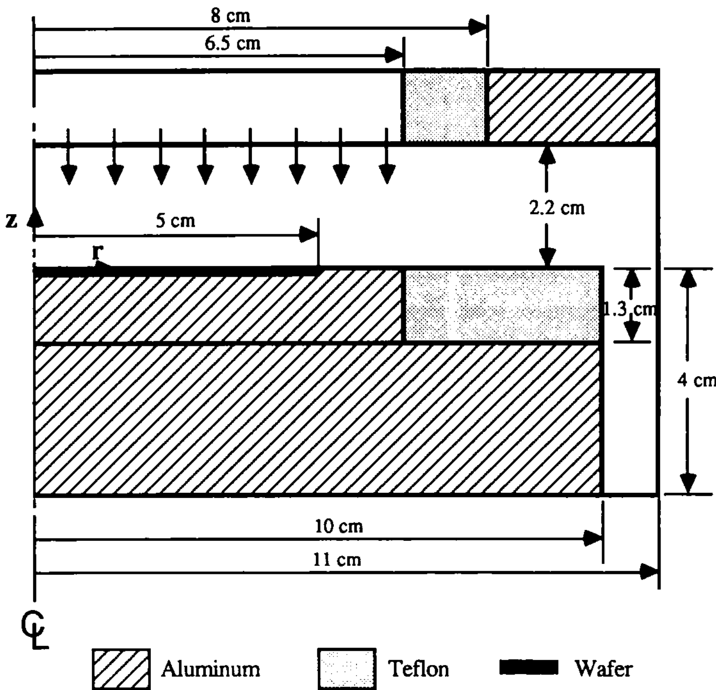

Fig. 2. Schematic of the axisymmetric parallel-plate single-wafer reactor studied.

function of duty cycle was studied. The performance of a power-modulated plasma reactor was compared to that of a continuous wave (CW) reactor.

2. MODEL FORMULATION

A schematic of the parallel-plate single-wafer plasma etching reactor is shown in Fig. 2. The reactor design and dimensions correspond to those of our experimental system. The feed gas enters uniformly through a showerhead arrangement in the upper electrode which can be powered by a continuous wave or a power-modulated source. The spent gas is pumped radially outwards. The wafer is placed on the lower grounded electrode. It was assumed that the wafer is in a good thermal contact with the lower electrode and the metal support. Therefore, the temperatures of the wafer, the lower electrode, and the metal support were taken to be identical.

The wafer temperature is an important issue in plasma etching. Production etchers use elaborate cooling systems (e.g., He chuck) to control the wafer temperature. Laboratory systems use thermally conductive grease.

Table I. Reaction Scheme Used for CF_4 Plasma Etching of Silicon[a]

A. Homogeneous (gas-phase) reactions

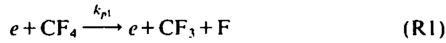

$$e + CF_4 \xrightarrow{k_{r1}} e + CF_3 + F \qquad (R1)$$

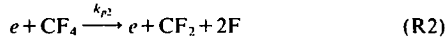

$$e + CF_4 \xrightarrow{k_{r2}} e + CF_2 + 2F \qquad (R2)$$

$$F + CF_2 \xrightarrow{k_{v1}} CF_3 \qquad (R3)$$

$$F + CF_3 \xrightarrow{k_{v2}} CF_4 \qquad (R4)$$

$$CF_3 + CF_3 \xrightarrow{k_{v3}} C_2F_6 \qquad (R5)$$

B. Surface reactions

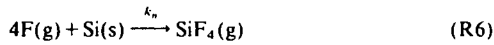

$$4F(g) + Si(s) \xrightarrow{k_n} SiF_4(g) \qquad (R6)$$

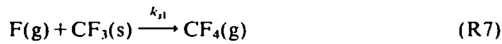

$$F(g) + CF_3(s) \xrightarrow{k_{s1}} CF_4(g) \qquad (R7)$$

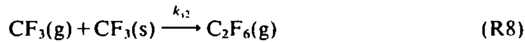

$$CF_3(g) + CF_3(s) \xrightarrow{k_{s2}} C_2F_6(g) \qquad (R8)$$

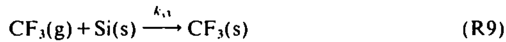

$$CF_3(g) + Si(s) \xrightarrow{k_{s3}} CF_3(s) \qquad (R9)$$

[a] k_j represents the rate coefficient of the corresponding reaction. (s) denotes surface species, e.g., $CF_3(s)$ denotes CF_3 adsorbed on the surface.

When precautions are not taken, the wafer temperature can indeed rise during etching with a concomitant increase in etch rate.[17]

The CF_4 plasma etching of silicon was taken as an example system for analysis. The reactor was assumed symmetric (plasma confined between the equal-area electrodes), operating at high pressure (~1 torr) and high frequency (13.56 MHz), above the ion sheath transit frequency. Under these conditions ion-assisted etching is relatively unimportant. Hence emphasis was placed on the neutral radical chemistry in the gas phase and on the wafer surface, since the focus of this paper is to examine the effect of power modulation on the radical transport and chemistry, and in turn the effect on etch rate and uniformity. The gas-phase (volume) and surface reactions believed to be important in the CF_4 plasma etching of silicon[18,19] are listed in Table I.

2.1. Radical Transport and Reaction

In order to obtain the gas velocity, temperature, and radical concentration distributions, one needs to solve the overall mass continuity, momentum, energy, and species mass balance equations. The following approximations were made to streamline the computational effort:

(a) The flow is in the continuum regime (Knudsen number $Kn = \lambda/d \ll 1$), it is laminar, and the fluid is Newtonian. This assumption is well satisfied for the conditions examined.

(b) The standard Boussinesq approximation can be used, i.e., the gas density can be assumed constant (ρ_0) except for the buoyancy term in the momentum equation [last term of Eq. (2) below]. This assumption is reasonable as the temperature gradients in the system are relatively small (see Results).

(c) Gas heating due to homogeneous chemical reactions and electron-impact reactions are neglected; the gas is heated primarily through heat transfer from the walls. It is realized that some gas heating by the plasma will inevitably occur, but this is difficult to estimate. We are currently performing direct simulation Monte Carlo (DSMC) studies of plasma transport (albeit in a low-pressure gas), which accounts for gas heating naturally.

(d) The fluid can be approximated as an ideal gas.

(e) Mass transport in a "dilute" solution is assumed due to the small dissociation of the parent gas (see Results). This implies essentially binary diffusion of radicals in a sea of CF_4. Also, because of the small degree of dissociation of the parent gas, gas velocity changes due to change in the number of moles are neglected.

(f) Because gas heating by the plasma is unimportant [assumption (c)], and the change in the number of moles is negligible, the velocity and temperature distributions are not affected by any power modulation applied to the plasma. Power modulation renders the radical concentration time-dependent, but the velocity and temperature profiles remain time-independent.

(g) The reactor is axisymmetric. Therefore only two spatial dimensions (r, z) are important.

Based on the above assumptions the governing equations can be written as

Continuity

$$\nabla \cdot \mathbf{v} = 0 \tag{1}$$

Momentum balance

$$\rho_0 \mathbf{v} \cdot \nabla \mathbf{v} = \nabla \cdot \tau - \rho_0 \mathbf{g} \beta (T - T_0) \tag{2}$$

where τ is a tensor given by

$$\tau = -p\mathbf{I} + \mu[\nabla \mathbf{v} + (\nabla \mathbf{v})^{\mathrm{T}}]$$

$\mathbf{I}$ is the identity matrix and superscript T denotes the transpose of a matrix.

Energy balance (in terms of temperature)

$$\rho C_p(\mathbf{v} \cdot \nabla T) = \nabla \cdot (\kappa \nabla T) \tag{3}$$

Mass balance

$$\frac{\partial C_i}{\partial t} + \mathbf{v} \cdot \nabla C_i = \nabla \cdot (D_{i,CF_4} C_T \nabla x_i) + R_i \tag{4}$$

Four species, $i = F$, CF_2, CF_3, and CF_4, were included in the calculation. Here R_i is the net production rate of species i. For example, the net production rate of F is given by

$$R_F = (k_{p1} n_e + 2k_{p2} n_e) C_{CF_4} - k_{v1} C_F C_{CF_2} - k_{v2} C_F C_{CF_3} \tag{5}$$

In the above equations, $\mathbf{v}$ is the gas velocity vector, T and T_0 are the gas temperature and a reference temperature, respectively, p is the dynamic pressure, C_i and x_i are the molar concentration and mole fraction of species i, respectively, C_T is the total gas molar concentration, $\mathbf{g}$ is the gravitational acceleration vector, μ is the gas viscosity, and β is the thermal expansion coefficient defined by

$$\beta = -\frac{1}{\rho}\left(\frac{\partial \rho}{\partial T}\right)_p \tag{6}$$

Furthermore, ρ and ρ_0 are the gas densities at T and T_0, respectively, C_p is the constant-pressure heat capacity, κ is the gas thermal conductivity, D_{i,CF_4} is the binary diffusivity of species i in CF_4, and n_e is the electron density.

In Eq. (5) the terms in parenthesis account for F production by electron-impact dissociation of the parent gas (reactions R1 and R2 in Table I), while the last two terms account for F loss by volume recombination reactions with CF_2 and CF_3 radicals (reactions R3 and R4 in Table I). The mole fraction of the reaction product (SiF_4) can be obtained from the constraint that the mole fractions of all species should sum up to unity.

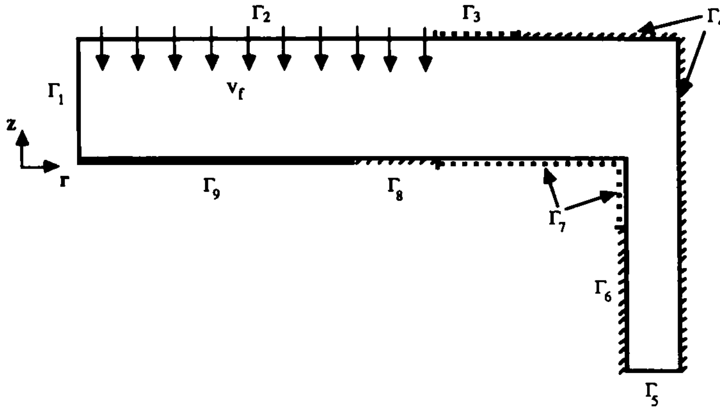

Fig. 3. Boundary conditions are applied on boundaries Γ_1 to Γ_9 (see also Fig. 2).

2.2. Boundary and Initial Conditions

Boundary conditions were applied on the boundaries designated by Γ_i ($i=1$–9) as shown in Fig. 3. The boundary conditions for velocity and temperature are as follows:

$$\Gamma_{1,5} \qquad v_r=0, \quad \frac{\partial v_z}{\partial n}=0, \quad \frac{\partial T}{\partial n}=0 \tag{7}$$

$$\Gamma_2 \qquad v_r=0, \quad v_z=-v_f, \quad \kappa\frac{\partial T}{\partial n}=\rho_0 v_f C_p(T_f-T) \tag{8}$$

$$\Gamma_{3,7} \qquad v_r=0, \quad v_z=0, \quad \frac{\partial T}{\partial n}=0 \tag{9}$$

$$\Gamma_4 \qquad v_r=0, \quad v_z=0, \quad T=T_w \tag{10}$$

$$\Gamma_{6,8,9} \qquad v_r=0, \quad v_z=0, \quad T=T_s \tag{11}$$

Here, v_r and v_z are the velocity components in the radial and axial directions, respectively, v_f is the inlet velocity of the feed gas, T_f, T_s, and T_w are the feed, wafer, and reactor wall temperatures, respectively; n denotes the direction of the outward normal to the boundary.

A symmetry condition was applied along the reactor axis Γ_1, a uniform velocity and a Dankwerts' condition[20] on temperature at the showerhead inlet Γ_2, adiabatic walls along the Teflon surfaces Γ_3 and Γ_7, constant temperature on the wafer Γ_9, substrate electrode Γ_8 and reactor wall Γ_6, and reactor outer metal wall Γ_4, and Dankwerts' condition at the exit, Γ_5. In

addition, the no-slip condition for the velocity field was assumed on all solid surfaces.

The boundary conditions for the radical concentration are

$$\Gamma_{1,3,4,5,6,7,8} \qquad \frac{\partial x_i}{\partial n}=0 \tag{12}$$

$$\Gamma_2 \qquad D_{i,\mathrm{CF_4}}C_T\frac{\partial x_i}{\partial n}=v_f(C_{if}-C_i) \tag{13}$$

$$\Gamma_9 \quad \begin{cases} -D_{\mathrm{F,CF_4}}C_T\dfrac{\partial x_\mathrm{F}}{\partial n}=k_{s1}C_\mathrm{F}\theta+k_nC_\mathrm{F}(1-\theta) & (14)\\[2ex] \dfrac{\partial x_{\mathrm{CF_2}}}{\partial n}=0 & (15)\\[2ex] -D_{\mathrm{CF_3,CF_4}}C_T\dfrac{\partial x_{\mathrm{CF_4}}}{\partial n}=k_{s2}C_{\mathrm{CF_3}}\theta+k_{s3}C_{\mathrm{CF_3}}(1-\theta) & (16)\\[2ex] D_{\mathrm{CF_4,CF_4}}C_T\dfrac{\partial x_{\mathrm{CF_4}}}{\partial n}=k_{s1}C_\mathrm{F}\theta & (17) \end{cases}$$

where θ is the fraction of the Si surface covered by CF_3, given as

$$\theta=\frac{k_{s3}C_{\mathrm{CF_3}}}{(k_{s2}+k_{s3})C_{\mathrm{CF_3}}+k_{s1}C_\mathrm{F}} \tag{18}$$

C_{if} is the feed concentration for the ith species. In the calculation, pure CF_4 was used as feed gas. A symmetry condition was applied at the reactor axis Γ_1, Dankwerts' conditions at the showerhead Γ_2 and reactor exit Γ_5, the species flux was equated to the reaction rate on the wafer Γ_9, and no reaction was assumed on the rest of the solid surfaces Γ_3, Γ_4, and Γ_6-Γ_8. The initial condition for the concentration distributions was chosen as

$$t=0, \qquad C_{\mathrm{CF_4}}=C_{T,0}=\frac{p_0}{R_gT_0}, \qquad C_i=0 \quad (i=\mathrm{F, CF_2, CF_3}) \tag{19}$$

where $C_{T,0}$ is the initial total gas concentration in the reactor, and R_g is the universal gas constant.

2.3. Electron Density

When the power delivered to the plasma is modulated, the electron energy and density modulate accordingly. Modulation in the electron energy distribution function (EEDF) causes the rate coefficients of electron-impact

reactions to be time-dependent. High threshold energy processes such as dissociation depend on the tail of the EEDF which, for the conditions of interest, responds on a nanosecond time scale.[21] On the other hand, the electron density buildup and decay may respond on a time scale of 10–100 μs.[22,23] These time scales are much shorter than typical values of the period of power modulation ($T_p = 1$–1000 ms). Hence, a square wave modulation of the electron density and electron-impact rate coefficients can be assumed following the excitation waveform shown in Fig. 1. In mathematical terms,

continuous wave $$n_e = n_{c0} \tag{20}$$

power modulation $$n_e = n_{e0}\left[\sum_{j=0}^{N_p}\left[U(T-jT_p) - U(T-(j+f_d)T_p)\right]\right] \tag{21}$$

for $jT_p \leq T < (j+1)T_p$, $j = 0, 1, \ldots, N_p$. In a power-modulated plasma, n_{e0} corresponds to the power level during the plasma-on fraction of the cycle and N_p is the number of cycles. $U(x)$ is a step function defined as $U(x) = 1$ for $x \geq 0$ and $U(x) = 0$ for $x < 0$. T_p is the pulse period, and f_d is the duty cycle defined as the ratio of the plasma-on time during one cycle to the period T_p (Fig. 1a). T_p used in the calculations varied from 0.001 to 0.2 s. An expression analogous to Eq. (21) was used for the case of Fig. 1b.

Equations (20) and (21) are written under the assumption of a spatially uniform electron density. The electron density distribution in an electropositive gas (e.g., argon) is set by ambipolar diffusion, which results in a Bessel-like profile in the radial direction and a cosine-like profile in the axial direction. In electronegative gases, the space charge fields are partly neutralized by the negative ions and the electron diffusivity is closer to the free diffusion value (which is much higher than the ambipolar diffusivity). Due to the high electron diffusivity, the electron density profiles are flatter in electronegative gases, such as CF_4, compared to electropositive gases.

2.4. Etch Rate and Uniformity

Once the radical concentration distribution is found, the etch rate r_n and uniformity can be calculated. The radially dependent etch rate of silicon is given by (see reaction R6 of Table I)

$$r_n = \tfrac{1}{4}k_n(1-\theta)C_F \tag{22}$$

The uniformity index UI is defined as

$$\mathrm{UI} = \frac{r_{n,\max} - r_{n,\min}}{2r_{\mathrm{avg}}} \tag{23}$$

Table II. Reaction Rate Coefficients and Transport Properties[a]

$k_{p1} = 6 \times 10^{-10}\ \mathrm{cm^3/s}$
$k_{p2} = 14 \times 10^{-10}\ \mathrm{cm^3/s}$
$k_{v1} = 4.741 \times 10^{11}\ \mathrm{cm^3/mol\text{-}s}$ (at 1.0 torr)
$k_{v2} = 9.039 \times 10^{12}\ \mathrm{cm^3/mol\text{-}s}$ (at 1.0 torr)
$k_{v3} = 4.787 \times 10^{12}\ \mathrm{cm^3/mol\text{-}s}$ (at 1.0 torr)
$k_{s1} = 4.17(T_s)^{0.5}\ \mathrm{cm/s}$
$k_{s2} = 0.438(T_s)^{0.5}\ \mathrm{cm/s}$
$k_{s3} = 0.876(T_s)^{0.5}\ \mathrm{cm/s}$
$k_n = 104.3(T_s)^{0.5} \exp(-1258/T_s)\ \mathrm{cm/s}$
$D_{F,CF_4} = 2.42 \times 10^{-2} T^{1.5}/p\ \mathrm{cm^2/s}$
$D_{CF_2,CF_4} = 1.30 \times 10^{-2} T^{1.5}/p\ \mathrm{cm^2/s}$
$D_{CF_3,CF_4} = 1.09 \times 10^{-2} T^{1.5}/p\ \mathrm{cm^2/s}$
$D_{CF_4,CF_4} = 9.51 \times 10^{-3} T^{1.5}/p\ \mathrm{cm^2/s}$
$\mu = 1.016 \times 10^{-5} T^{0.5}\ \mathrm{g/cm\text{-}s}$
$\kappa = -1.692 \times 10^{-5} + 2.16 \times 10^{-7} T - 4.54 \times 10^{-11} T^2 + 5.04 \times 10^{-15} T^3\ \mathrm{cal/cm\text{-}s\text{-}K}$
$C_p = 3.339 + 4.838 \times 10^{-2} T - 3.882 \times 10^{-5} T^2 + 1.078 \times 10^{-8} T^3\ \mathrm{cal/mol\text{-}K}$
$\beta = 0.00367\ \mathrm{K^{-1}}$

[a] p in torr, T_s and T in K.

with the average etch rate calculated by

$$r_{\mathrm{avg}} = \frac{2 \int_0^R r_n r\, dr}{R^2} \tag{24}$$

$r_{n,\max}$ and $r_{n,\min}$ are the maximum and minimum etch rates on the Si wafer having radius R. The lower the value of UI, the better the etch uniformity.

A list of the reaction rate coefficients and transport properties used in this work is shown in Table II. The rate coefficients were taken from Edelson and Flamm[18] and Plumb and Ryan.[19] Heat capacity data was obtained from Reid.[24] Viscosity, thermal conductivity, and binary diffusivities were estimated using the Chapman–Enskog kinetic theory.[25]

3. METHOD OF SOLUTION

The finite element method was employed to solve the conservation equations, subject to the initial and boundary conditions specified above. Assumptions (c) and (e) permit the decoupling of the momentum and energy balance equations from the species mass balance equations. Hence the gas velocity and temperature profiles were computed first by solving the coupled Eqs. (1)–(3). The resulting distributions were used in the mass balance equations [Eqs. (4)] to determine the spatiotemporal variations of species concentration. The penalty-function formulation for incompressible flow[26]

Table III. Operating Conditions and Range Examined

Quantity	Base value	Range
Flow rate, Q_0 (sccm)	100	25–500
Gas pressure, p_0 (torr)	1.0	1.0–2.0
Wafer temperature, T_s (K)	350	350–500
Pulse period, T_p (s)	0.01	0.001–0.2
Duty cycle, f_d	50%	10–100%
Reference, feed, and reactor wall temperatures, T_0, T_f, T_w (K)	298	N.A.
Electron density, n_{e0} (cm^{-3})	10^{10}	N.A.

was employed to replace the dynamic pressure by

$$p = -\lambda \nabla \cdot \mathbf{v} \tag{25}$$

with λ being a large parameter. This method eliminates the pressure p from the momentum balance equation and makes the equation of incompressibility [Eq. (1)] unnecessary.

A nonuniform spatial grid was used, with finer mesh in places where the dependent variables were expected to have steeper gradients. Also, a nonuniform step size was used for time integration of the mass balance equations. Preliminary numerical experiments were conducted to select the optimum size of the grid and time step. The convergence to periodic steady state was detected by the following criterion:

$$\xi_{ss} = \left\{ \sum_{j=1}^{NT} \left(\left(\frac{r_{\mathrm{avg},j}}{\bar{r}_{\mathrm{avg}}} \right)_{(l+1)T_p} - \left(\frac{r_{\mathrm{avg},j}}{\bar{r}_{\mathrm{avg}}} \right)_{lT_p} \right)^2 \right\}^{1/2} \Big/ \mathrm{NT} \tag{26}$$

where $r_{\mathrm{avg},j}$ is the space-averaged etch rate at time step j. $\bar{r}_{\mathrm{avg}}$ is the time-averaged value of $r_{\mathrm{avg},j}$ over one pulse period, NT is the number of time steps per cycle, and ξ_{ss} is a user-specified error tolerance.

Calculations were performed on a Cray Y-MP supercomputer at the Pittsburgh Supercomputer Center and a VAX computer. The CPU time varied with operating conditions (flow rate, pulse period, etc.) and initial condition. For a power-modulated plasma simulation using $T_p = 0.01$ s, a flow rate of 100 sccm, and NT = 200, it took 1.2 CPU hours of the Cray C90 to reach the periodic steady state with $\xi_{ss} = 10^{-6}$.

4. RESULTS AND DISCUSSION

Radical concentration distributions, etch rate, and uniformity were calculated for continuous wave (CW) and power-modulated plasma etching. The plasma was assumed to be confined extending up to the electrode edge ($r = 6.5$ cm in Fig. 2). This is a good assumption for a symmetric (equal-area electrodes) system operating at relatively high pressure (1 torr). Base values for reactor operating conditions and the range examined are shown in Table III. The power delivered to the CW system was such as to obtain

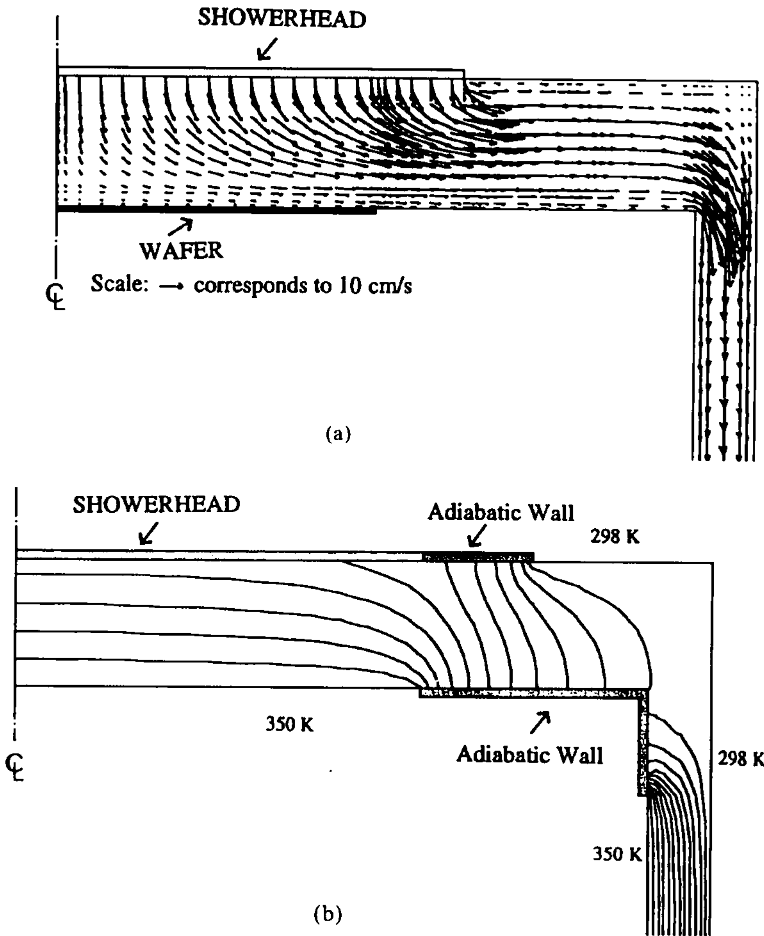

Fig. 4. (a) Gas velocity vector plot. Gas enters uniformly through the porous boundary Γ_2 and exits through Γ_5 (Fig. 3). Velocity is zero on all solid surfaces. (b) Temperature contour plot. Boundaries Γ_6, Γ_8, and Γ_9 (Fig. 3) are kept at 350 K. Boundary Γ_4 is at 298 K. Heat flux through Γ_3 and Γ_7 is zero. Both (a) and (b) are for a CW plasma reactor at base case conditions (Table III).

an electron density of $n_{e0} = 10^{10}$ cm^{-3}. A fraction of this power (equal to the duty cycle) was delivered to the power-modulated system. Calculations were performed using the base values of Table III, unless noted otherwise.

Figure 4 shows the gas velocity (Fig. 4a) and temperature (Fig. 4b) distributions in the reactor. CF_4 feed gas enters uniformly through the

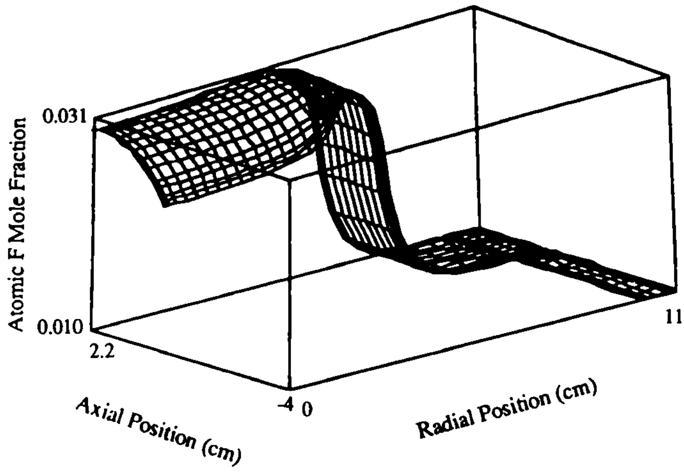

Fig. 5. Fluorine radical (F) mole fraction in a CW plasma. Base case conditions (Table III).

< 0.010 I 11